

Real-Time Power System Frequency and Phasors Estimation Using Recursive Wavelet Transform

Jinfeng Ren, *Student Member, IEEE*, and Mladen Kezunovic, *Fellow, IEEE*

Abstract—Phasor frequency, magnitude, and angle describing a sinusoidal signal are widely used as critical variables in algorithms and performance indices in many power system applications, such as the protection relaying and state monitoring. This paper proposes a novel approach for estimating the phasor parameters, namely frequency, magnitude, and angle in real time based on a newly constructed recursive wavelet transform. This algorithm is capable of estimating the phasor parameters in a quarter cycle of an input signal. It features fast response and achieves high accuracy over a wide range of frequency deviations. The signal sampling rate and data window size can be selected to meet desirable applications requirements, such as fast response, high accuracy, and low computational burden. Besides, an approach for eliminating a decaying dc component, which has a significant impact on estimating phasors, is proposed by using a recursive wavelet transform. Simulation results demonstrate that the proposed methods achieve good performance.

Index Terms—Decaying dc component, frequency, phasor, phasor parameter estimation, recursive wavelet transform (RWT), sinusoidal signal, total vector error (TVE).

I. INTRODUCTION

IN POWER systems, many applications need real-time measurements of frequency and other phasor parameters of voltage and current signals for the purpose of monitoring, control, and protection. Power system frequency as a key property of a phasor can be indicative of system abnormal conditions and disturbances. The phasor frequency, amplitude, and phase angle are critical variables used by many algorithms. How to rapidly and accurately estimate frequency and other phasor parameters is still a contemporary topic of research interest.

Discrete Fourier transform (DFT) is widely used as a filtering algorithm for estimating fundamental frequency phasors [1], [2]. The conventional DFT algorithm achieves excellent performance when the signals contain only fundamental frequency and integer harmonic frequency components. Since, in most cases, the currents contain decaying dc components may introduce fairly large errors in the phasor estimation [3], [4].

A variety of techniques for the real-time estimation of power system frequency has been developed and evaluated in past two decades. As an example, DFT has been extensively applied to

extract frequency due to its low computation requirement. However, the implicit data window in the DFT approach causes errors when frequency deviates from the nominal value [5]. To improve the performance of DFT-based approaches, some adaptive methods based on the feedback loop by tuning the sampling interval [6], adjusting the data window length [7], changing the nominal frequency used in DFT iteratively [5], correcting the gains of orthogonal filters [8], and tuning the weighted factor [9] recursively are proposed. Due to the inherent limitation in DFT, at least one cycle of analyzed signal is required, which hardly meets the demand of high-speed response for protection schemes. A method using three consecutive samples of the instantaneous input signal is discussed in [10]. The noise and zero crossing issue may bring large errors to this method. On the basis of the stationary signal model, some nonlinear curve fitting techniques, including extended Kalman filter [11] and recursive least-squares algorithm [12], are adopted to estimate the fundamental frequency. The accuracy is only reached in a narrow range around the nominal frequency due to the truncation of Taylor series expansions of nonlinear terms. Some artificial-intelligence techniques, such as genetic algorithm [13] and neural networks [14], have been used to achieve precise frequency estimation over a wide range with fast response. Although better performance can be achieved by these optimization techniques, the implementation algorithm is more complex and intense in computation.

Many techniques have been proposed to eliminate the impact of decaying dc components in phasor estimation. A digital mimic filter-based method was proposed in [15]. This filter features high-pass frequency response which results in bringing high-frequency noise to the outcome. It performs well when its time constant matches the time constant of the exponentially decaying component. Theoretically, the decaying component can be completely removed from the original waveform once its parameters can be obtained. Based on this idea, [16] and [17] utilize additional samples to calculate the parameters of the decaying component. Reference [18] uses the simultaneous equations derived from the harmonics. The effect of dc components by DFT is eliminated by using the outputs of even-sample-set and odd-sample-set [19]. Reference [20] hybridizes the partial sum-based method and least-squares-based method to estimate the dc offsets parameters. A new Fourier algorithm and three simplified algorithms based on Taylor expansion were proposed to eliminate the decaying component in [21]. In [22], the author estimates the parameters of the decaying component by using the phase-angle difference between voltage and current. This method requires both voltage and current inputs. As a result, it is not applicable to the current-based protection schemes.

Manuscript received October 05, 2009; revised March 19, 2010; accepted March 23, 2011. Date of publication May 05, 2011; date of current version June 24, 2011. Paper no. TPWRD-00749-2009.

The authors are with the Department of Electrical and Computer Engineering, Texas A&M University, College Station, TX 77843-3128 USA (e-mail: j.f.ren@neo.tamu.edu; kezunov@ece.tamu.edu).

Color versions of one or more of the figures in this paper are available online at <http://ieeexplore.ieee.org>.

Digital Object Identifier 10.1109/TPWRD.2011.2135385

The recursive wavelet approach was introduced in protective relaying for a long time [23]–[25]. The improved model with single-direction recursive equations is more suitable for the application to real-time signal processing [24]. The band energy of any center frequency can be extracted through recursive wavelet transform (RWT) with moderately low computation burden.

A new mother wavelet with recursive formula is constructed in our paper. The RWT-based real-time frequency and phasor estimation and decaying dc component elimination scheme is proposed. The algorithm can produce accurate phasor outputs in a quarter cycle of an input signal. It responds quite fast although the time delay brought by prefiltering may be prominent. The convergence analysis indicates that the higher sampling rate one uses, the shorter the data window size that the computation needs, and vice-versa. The sampling rate has barely had an effect on the accuracy once it reaches 50 samples per cycle (i.e., 3 kHz for a 60-Hz power system) or higher. Besides, a method for removing the decaying dc component, which affects the performance of extracting the fundamental frequency component, is proposed by using the RWT. Analysis indicates that the computational burden is moderate. Performance test results including static, dynamic, transient, and noise tests demonstrate the advantages of the proposed method.

II. RECURSIVE WAVELET TRANSFORM

The mother wavelet function is defined as a function $\psi(t)$ which satisfies the admissibility condition

$$C_{\Psi} = \int_{-\infty}^{+\infty} \frac{|\Psi(\omega)|^2}{|\omega|} d\omega < \infty$$

$$\text{i.e., } \Psi(\omega)|_{\omega=0} = \int_{-\infty}^{+\infty} \psi(t) dt = 0$$

where $\Psi(\omega)$ is the Fourier transform of $\psi(t)$.

A set of wavelet functions can be derived from $\psi(t)$ by dilating and shifting the mother wavelet, as will be given

$$\psi_{a,b}(t) = a^{-1/2} \cdot \psi\left(\frac{t-b}{a}\right), a > 0$$

where a and b are the scaling (dilation) factor and time shifting (translation) factor, respectively.

A “good” wavelet is such a function that meets the admissibility condition and has a small time–frequency window area [26]. We construct a mother wavelet function as expressed as follows:

$$\psi(t) = \left(\frac{\sigma t}{2} + \frac{\sigma^2 t^2}{2} + \frac{\sigma^3 t^3}{3}\right) e^{(\sigma + j\omega_0)t} u(-t).$$

And we designate function $\psi_1(t) = \psi^*(-t)$

$$\psi_1(t) = \left(-\frac{\sigma t}{2} + \frac{\sigma^2 t^2}{2} - \frac{\sigma^3 t^3}{3}\right) e^{(-\sigma + j\omega_0)t} u(t).$$

Its frequency-domain expression obtained by Fourier transform is given in the following expression:

$$\Psi(\omega) = \frac{\sigma(\omega_0 - \omega)^2 - 3\sigma^3}{2 \cdot [\sigma + j(\omega_0 - \omega)]^4}.$$

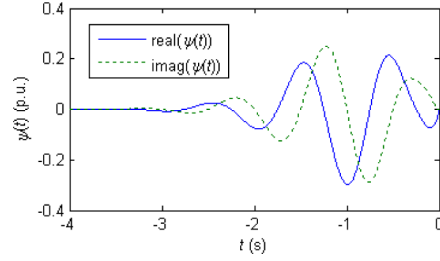


Fig. 1. Time-domain waveforms of $\psi(t)$.

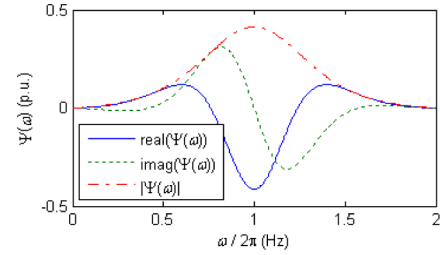


Fig. 2. Frequency-domain waveforms of $\Psi(\omega)$.

Setting $\sigma = 2\pi/\sqrt{3}$, $\omega_0 = 2\pi$ makes the wavelet function $\psi(t)$ admissible (i.e., $\Psi(\omega)|_{\omega=0} = 0$).

One can see that the newly constructed wavelet is a complex function whose time- and frequency-domain expressions contain real and imaginary parts. Figs. 1 and 2 give the time- and frequency-domain waveforms of $\psi(t)$ and $\Psi(\omega)$, respectively. Some performance parameters can be calculated to specify a wavelet function [26]. The time-domain center t^* and window radius Δt of wavelet function $\psi(t)$ are -0.99 s and 0.40 s, respectively. As one can see in Fig. 2, it features a band-pass filter with the frequency-domain center ω^* and band radius $\Delta\omega$ of 2π rad and 1.38 rad. One advantage of the wavelet transform is that the quality factor Q , defined as the ratio of frequency center ω^* and bandwidth $2\Delta\omega$, stays constant as the observation scale varies. For $\Psi(\omega)$, $Q = \omega^*/2\Delta\omega = 2.27$. The complex wavelet exhibits good time-frequency localization characteristics. Its time-frequency window area S , defined as a product of time window width $2\Delta t$ and frequency bandwidth $2\Delta\omega$, is 2.23 rad·s.

To obtain the center frequency f_c of the band-pass filter, which is defined as the frequency in which the function reaches the maximum magnitude, we have the Fourier transform for the dilated wavelet function $\psi(t/a)$

$$\Psi(a\omega) = \frac{\sigma(\omega_0 - a\omega)^2 - 3\sigma^3}{2 \cdot [\sigma + j(\omega_0 - a\omega)]^4}.$$

$|\Psi(a\omega)|$ reaches the maximum value when $a \cdot \omega = \omega_0$, that is, $a \cdot 2\pi \cdot f_c = 2\pi$. Thus, we have $f_c = 1/a$. That is, the scale factor a is reciprocal to the center frequency f_c of the band-pass filter.

Since the wavelet function $\psi(t)$ is anticausal, which has zeros for all positive time, the wavelet transform coefficient in scale a for a given causal signal $x(t)$ can be expressed as

$$W_{x(t)}(a, b) = a^{-1/2} \int_0^b x(t) \cdot \psi\left(\frac{t-b}{a}\right)^* dt, t > 0. \quad (1)$$

Let ΔT be the sampling period, and n and k be integers. Then, $t = n\Delta T$, $b = k\Delta T$. With the observing frequency $f = 1/a$, (1) can be expressed discretely

$$\begin{aligned} W_{x(n\Delta T)}(f, k\Delta T) &= \Delta T \sqrt{f} \sum_{n=1}^{\infty} x(n\Delta T) \cdot \psi^*(f(n\Delta T - k\Delta T)) \\ &= \Delta T \sqrt{f} \sum_{n=1}^{\infty} x(n\Delta T) \cdot \psi_1(f(k\Delta T - n\Delta T)). \end{aligned}$$

The formula just shown can be expressed by using convolution

$$W_{x(n\Delta T)}(f, k\Delta T) = \Delta T \sqrt{f} [x(n\Delta T) * \psi_1(fn\Delta T)].$$

Taking the z -transform on both sides, we have

$$W_x^z(f, Z) = \Delta T \sqrt{f} [X(Z) \cdot \Psi_1(Z)] \quad (2)$$

where $W_x^z(f, Z)$, $X(Z)$, and $\Psi_1(Z)$ are z -transforms of discrete sequences $W_{x(n\Delta T)}(f, k\Delta T)$, $x(n\Delta T)$, and $\psi_1(fn\Delta T)$, respectively.

Based on the expression of wavelet function $\psi_1(t)$, we derive its discrete form in terms of observing frequency f

$$\begin{aligned} \psi_1(fn\Delta T) &= \left(-\frac{\sigma fn\Delta T}{2} + \frac{\sigma^2 (fn\Delta T)^2}{2} - \frac{\sigma^3 (fn\Delta T)^3}{3} \right) \\ &\quad \cdot e^{(-\sigma + j\omega_0)(fn\Delta T)} u(fn\Delta T). \end{aligned}$$

Its z -transform is expressed as follows:

$$\Psi_1(Z) = \sum_{n=0}^{\infty} \psi_1(fn\Delta T) \cdot Z^{-n}.$$

Denoting $\alpha = e^{-f\Delta T(\sigma - j\omega_0)}$, we obtain the expression for $\Psi_1(Z)$

$$\Psi_1(Z) = \frac{\lambda_1 z^{-1} + \lambda_2 z^{-2} + \lambda_3 z^{-3}}{1 + \beta_1 z^{-1} + \beta_2 z^{-2} + \beta_3 z^{-3} + \beta_4 z^{-4}} \quad (3)$$

where

$$\begin{aligned} \lambda_1 &= \alpha \cdot \left[\frac{-\sigma f \Delta T}{2} + \frac{(\sigma f \Delta T)^2}{2} - \frac{(\sigma f \Delta T)^3}{3} \right] \\ \lambda_2 &= \alpha^2 \cdot \left[\frac{\sigma f \Delta T - 4 \cdot (\sigma f \Delta T)^3}{3} \right] \\ \lambda_3 &= \alpha^3 \cdot \left[\frac{-\sigma f \Delta T}{2} - \frac{(\sigma f \Delta T)^2}{2} - \frac{(\sigma f \Delta T)^3}{3} \right] \\ \beta_1 &= -4\alpha \\ \beta_2 &= 6\alpha^2 \\ \beta_3 &= -4\alpha^3 \\ \beta_4 &= \alpha^4. \end{aligned}$$

From (2) and (3), we obtain

$$\begin{aligned} W_x^z(Z) &= \Delta T \sqrt{f} \cdot X(Z) \\ &\quad \times (\lambda_1 z^{-1} + \lambda_2 z^{-2} + \lambda_3 z^{-3}) - W_x^z(Z) \\ &\quad \times (\beta_1 z^{-1} + \beta_2 z^{-2} + \beta_3 z^{-3} + \beta_4 z^{-4}). \end{aligned}$$

According to the properties of inversion of the z -transform, we obtain the recursive expression for discretely computing wavelet transform coefficients

$$\begin{aligned} W_{x(n\Delta T)}(f, k\Delta T) &= \Delta T \sqrt{f} \left[\lambda_1((k-1)\Delta T) + \lambda_2 x((k-2)\Delta T) \right. \\ &\quad \left. + \lambda_3 x((k-3)\Delta T) \right] \\ &\quad - \beta_1 W_{x(n\Delta T)}(f, (k-1)\Delta T) \\ &\quad - \beta_2 W_{x(n\Delta T)}(f, (k-2)\Delta T) \\ &\quad - \beta_3 W_{x(n\Delta T)}(f, (k-3)\Delta T) \\ &\quad - \beta_4 W_{x(n\Delta T)}(f, (k-4)\Delta T). \end{aligned} \quad (4)$$

In (4), f represents the observing center frequency which is reciprocal to the scale factor a . To extract the frequency band energy centered in 60 Hz, for instance, simply apply $f = 60$ to (4). One can notice that wavelet transform coefficients can be calculated recursively with the historical data. This type of wavelet transform is so-called the recursive wavelet transform (RWT). Compared with the RWT in [23] and [24], the proposed RWT requires the historical data and less computation; thus, it can be used in real-time applications.

III. FREQUENCY AND PHASOR ESTIMATION

As discussed in Section II, the recursive wavelet (RW) features a complex wavelet whose wavelet transform coefficients (real part and imaginary part) contain both phase and magnitude information of the input signal, based on which the algorithm for estimating the power system frequency and phasor is derived as follows.

A. RWT-Based Frequency and Phasor Estimation

Let us consider a discrete input signal that contains M th order harmonics with a sampling period ΔT

$$\begin{aligned} x(n) &= \sum_{m=1}^M A_m \cos(2\pi \cdot f_m \cdot n\Delta T + \varphi_m) \\ n &= 0, 1, 2, \dots \end{aligned} \quad (5)$$

where f_m , A_m , and φ_m represent the frequency, amplitude, and phase angle of the m th order harmonic, respectively. Denoting the absolute phase angle of the m th order harmonic at sample n as $\theta_m(n) = 2\pi \cdot f_m n\Delta T + \varphi_m$, one can see that frequency f_m represents the rate of change of θ_m . For simplicity, the sampling period ΔT is neglected when expressing variables for the rest of this paper.

To represent the input signal $x(n)$ in the time-frequency domain, apply RWT in scale a using (4). As derived in the Appendix we have the following expression:

$$\begin{aligned} W_{x(n)}(a, k) &= \sum_{m=1}^M u_m^c(a, f_m, k) \cdot x_m^c(k) \\ &\quad + \sum_{m=1}^M u_m^s(a, f_m, k) \cdot x_m^s(k), \\ k &= 0, 1, 2, \dots \end{aligned} \quad (6)$$

From (6), one can see that the wavelet transform coefficient $W_{x(n)}$ contains information on the input signal in both cosine form and sine form, denoted as x_m^c and x_m^s in (7a) and (7b) (given in the Appendix), respectively, multiplied by weighting factors, denoted as u_m^c and u_m^s in (8a) and (8b) (given in the Appendix), respectively.

Let \tilde{f}_m represent the initial estimate of frequency variable, and rewrite (8a) using the first-order Taylor series expansion. That is

$$\begin{aligned} u_m^c(a, f_m, k) &\cong u_m^c(a, \tilde{f}_m, k) + \left. \frac{du_m^c}{df_m} \right|_{\tilde{f}_m} \cdot \Delta f_m \\ &= u_m^c(a, \tilde{f}_m, k) + u_m^{c1}(a, \tilde{f}_m, k) \cdot \Delta f_m \\ u_m^{c1}(a, \tilde{f}_m, k) &= -2\pi\sqrt{a}\Delta T^2 \sum_{l=k/a}^0 l \sin(2\pi\tilde{f}_m a l \Delta T) \\ &\quad \cdot Q. \end{aligned} \quad (9a)$$

where $Q = \left[\sigma/2(l\Delta T) + \sigma^2/2(l\Delta T)^2 + \sigma^3/3(l\Delta T)^3 \right] \cdot e^{(\sigma - j\omega_0) \cdot l\Delta T}$.

For simplicity, denote $u_m^c(a, \tilde{f}_m, k)$ and $u_m^{c1}(a, \tilde{f}_m, k)$ as \tilde{u}_m^c and \tilde{u}_m^{c1} , respectively. Then, we rewrite the equation as follows:

$$u_m^c(a, f_m, k) \cong \tilde{u}_m^c + \tilde{u}_m^{c1} \cdot \Delta f_m.$$

Following the same procedures, we can rewrite (8b) as follows:

$$\begin{aligned} u_m^s(a, f_m, k) &\cong \tilde{u}_m^s + \tilde{u}_m^{s1} \cdot \Delta f_m \\ \tilde{u}_m^{s1} &= 2\pi\sqrt{a}\Delta T^2 \sum_{l=k/a}^0 l \cos(2\pi\tilde{f}_m a l \Delta T) \cdot Q. \end{aligned} \quad (9b)$$

Then, (6) can be expressed as follows:

$$\begin{aligned} W_{x(n)}(a, k) &\cong \sum_{m=1}^M [\tilde{u}_m^c \cdot \tilde{x}_m^c(k) + \tilde{u}_m^{c1} \cdot \tilde{x}_m^{c1}(k)] \\ &\quad + \sum_{m=1}^M [\tilde{u}_m^s \cdot \tilde{x}_m^s(k) + \tilde{u}_m^{s1} \cdot \tilde{x}_m^{s1}(k)] \end{aligned} \quad (10a)$$

where $\tilde{x}_m^{c1} = \tilde{x}_m^c \cdot \Delta f_m$ and $\tilde{x}_m^{s1} = \tilde{x}_m^s \cdot \Delta f_m$.

Applying RWT to $x(n)$ in a series of scales a_1, a_2, \dots, a_{4M} , we obtain a series of coefficients w_1, w_2, \dots, w_{4M} that can be expressed in (10a). Rewrite those equations in matrix form as shown in the equation at the bottom of the page. For simplicity, we represent the previous matrix in vector form. At sample k , we have the following equation:

$$W(k) \cong \tilde{U}(k) \cdot \tilde{X}(k). \quad (10b)$$

In (10b), the wavelet coefficient $W(k)$ can be calculated by using recursive (4). For weighting factor $\tilde{U}(k)$, it can be calculated with estimated frequency \tilde{f}_m using (8a) and (8b) and (9a) and (9b). Solving (10b), we obtain vector variable $\tilde{X}(k)$. Then, we can derive the following formula for Δf_m :

$$\Delta f_m = \frac{\tilde{x}_m^c(k) \cdot \tilde{x}_m^{c1}(k) + \tilde{x}_m^s(k) \cdot \tilde{x}_m^{s1}(k)}{(\tilde{x}_m^c(k))^2 + (\tilde{x}_m^s(k))^2}. \quad (11a)$$

After we estimate the frequency adjustment, update the frequency with $\tilde{f}_m + \Delta f_m$ and iterate the aforementioned approximation procedures until either the frequency change reaches the cutoff value; for example, $\varepsilon = 0.001$ Hz, or a maximum number of iterations denoted as L is performed. As a result, the real frequency can be estimated at the last iteration. Then, the amplitude A_m and phase angle φ_m can be estimated by the following equations:

$$A_m = \sqrt{\tilde{x}_m^c(k) + \tilde{x}_m^s(k)} \quad (11b)$$

$$\varphi_m = \theta_m(k) - 2\pi \cdot \tilde{f}_m \cdot k\Delta T \quad (11c)$$

where $\theta_m(k) = \cos^{-1} \tilde{x}_m^c(k)$ or $\theta_m(k) = \sin^{-1} \tilde{x}_m^s(k)$.

The flowchart as given in Fig. 3 illustrates the implementation procedures for the proposed frequency, magnitude, and phase estimation algorithm. In practice, a low-pass filter with appropriate cutoff frequency is applied for eliminating high-frequency components in voltage and current measurements. As a result, the order of harmonic components can be limited within the range of cutoff frequency. For example, if a third-order Butterworth low-pass filter with a cutoff frequency of 320 Hz is used to prefilter input signals, in this case, the maximum order of harmonics will be limited to five (i.e., $M = 5$). Generally, we select m multiples of the nominal frequency (i.e., $f_0 = 60$ Hz, m represents the order of harmonics as an initial estimate to start iterations. To achieve high accuracy, scale factors $[a_1, a_2, \dots, a_{4M}]$ are required to cover all of the frequency components of the signal being analyzed. Therefore, we select $a_m = 1/(f_0 \times (1 + (m-1)/4))$. Extensive simulations show that the proposed algorithm can converge to the real value within three iterations. It should be noted that if only the fundamental frequency component is of interest (i.e., only f_1 is taken into the iteration loop), the dimension of scale factors and weighting matrix will be reduced to $2M + 2$. Obviously, if the input signal only contains the fundamental frequency component, the solved variables x_m^c and x_m^s ($2 \leq m \leq M$) will be some numbers close to zero, and then the parameters of those harmonics are meaningless.

$$\begin{bmatrix} w_{a_1} \\ w_{a_2} \\ w_{a_3} \\ w_{a_4} \\ \vdots \\ w_{a_{4M}} \end{bmatrix} \cong \begin{bmatrix} \tilde{u}_{1,a_1}^c & \tilde{u}_{1,a_1}^{c1} & \tilde{u}_{1,a_1}^s & \tilde{u}_{1,a_1}^{s1} & \cdots & \tilde{u}_{M,a_1}^{s1} \\ \tilde{u}_{1,a_2}^c & \tilde{u}_{1,a_2}^{c1} & \tilde{u}_{1,a_2}^s & \tilde{u}_{1,a_2}^{s1} & \cdots & \tilde{u}_{M,a_2}^{s1} \\ \tilde{u}_{1,a_3}^c & \tilde{u}_{1,a_3}^{c1} & \tilde{u}_{1,a_3}^s & \tilde{u}_{1,a_3}^{s1} & \cdots & \tilde{u}_{M,a_3}^{s1} \\ \tilde{u}_{1,a_4}^c & \tilde{u}_{1,a_4}^{c1} & \tilde{u}_{1,a_4}^s & \tilde{u}_{1,a_4}^{s1} & \cdots & \tilde{u}_{M,a_4}^{s1} \\ \vdots & \vdots & \vdots & \vdots & \ddots & \vdots \\ \tilde{u}_{1,a_{4M}}^c & \tilde{u}_{1,a_{4M}}^{c1} & \tilde{u}_{1,a_{4M}}^s & \tilde{u}_{1,a_{4M}}^{s1} & \cdots & \tilde{u}_{M,a_{4M}}^{s1} \end{bmatrix} \cdot \begin{bmatrix} \tilde{x}_1^c \\ \tilde{x}_1^{c1} \\ \tilde{x}_1^s \\ \tilde{x}_1^{s1} \\ \vdots \\ \tilde{x}_M^{s1} \end{bmatrix}$$

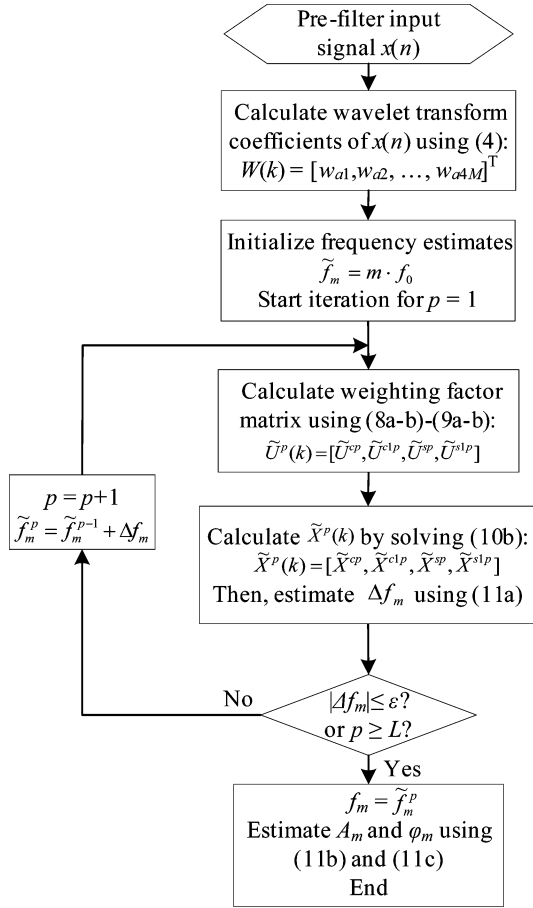


Fig. 3. Flowchart of the frequency, magnitude, and phase estimation.

B. Analysis of the Convergence Characteristics

The sampling rate and window length may affect the convergence characteristics because of two factors. One is that these formulae are derived based on the assumption that the error resulting from the discrete computation is negligible. Another is the error introduced by an inherent settling process in recursive equations. Besides, inappropriately selecting window size and sampling rate may cause the weighting factor matrix $\tilde{U}(k)$ singular.

To analyze the convergence characteristics, we define the window length l_s as the cycle of the nominal frequency, which is independent of the signal sampling frequency f_s defined as N times nominal frequency f_0 in Hertz. The variable l_s and f_s determine the number of samples N_s within a data window (i.e., $N_s = l_s \cdot f_s / f_0 = l_s \cdot N$). The total vector error (TVE) is used to measure the phasor accuracy [27]. Once the amplitude error ΔA_m (in percentage of the real value) and the phase error $\Delta \varphi_m$ (in degrees) are available, the expression for TVE is given by $TVE_m = \sqrt{(\Delta A_m)^2 + (\Delta \varphi_m / 0.573)^2}$, where 0.573 is the arcsine of 1% in degrees.

The signal model in (5) is used for the algorithm convergence analysis. In (5), we let $f_1 = 60$ Hz and $M = 5$; that is, the fundamental frequency component contained in the signal is 60 Hz and the frequency of harmonic noise is up to 300 Hz. Analysis results are given in Fig. 4, in which the dot represents the convergence while “x” stands for divergence. The results indicate

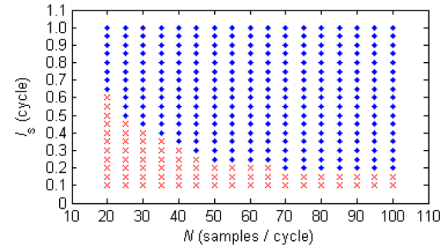
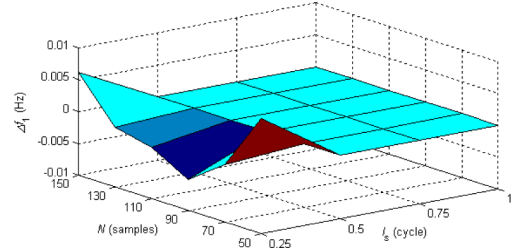
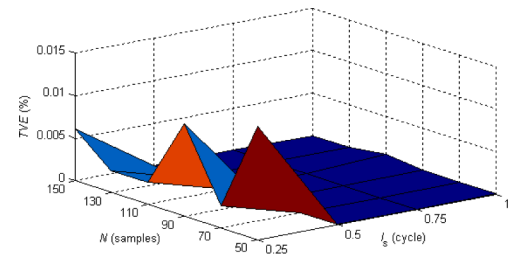


Fig. 4. Convergence analysis results.

Fig. 5. Estimate frequency error for $f_1 = 65$ Hz.Fig. 6. Estimate TVE for $f_1 = 65$ Hz.

that the window length can be shortened to 0.2 cycles if the sampling rate is 70 samples per cycle (i.e., 4.2 kHz) or higher.

Let us consider a case when the fundamental frequency deviates to 65 Hz and performs the algorithm to estimate frequency, magnitude, and phase. Relationships between frequency error, TVE, and two variables l_s and f_s , are shown in Figs. 5 and 6, respectively, in which the signal sampling rate is simulated from 50 to 150 samples per cycle while the window length changes from 0.25 to 1 cycle. One can see that the proposed algorithm achieves high accuracy and fast convergence. Simulations performed in Section V also show that for a broad range of frequency deviation, such as 55 Hz–65 Hz, the algorithm can converge to the real value within three iterations. Besides, the sampling rate has barely any effect on the accuracy once it reaches 50 samples per cycle (i.e., 3 kHz for the 60-Hz power system) or higher. Compared to the conventional DFT-based methods, this algorithm can shorten the window length to a quarter cycle.

Let us now consider the computation burden of the proposed algorithm. If we use 3 kHz sampling frequency and 0.25 cycle data window as the case performed in convergence analysis and performance tests, it approximately requires 6000 multiplications and 5796 summations. Only $68 \cdot (2M + 2) = 816$ multiplications and $51 \cdot (2M + 2) = 612$ summations are used for computing RWT coefficients $W_{2M+2}(12)$ (where $M = 5$), and $3 \cdot (2M + 2)^3 = 5184$ multiplications and summations for matrix inverse computation when three iterations are performed.

Weighting matrix $U(12)$ with various scales and frequencies can be calculated and stored in advance and can be accessed very fast by using a table lookup method. Some mathematical techniques, such as Chelosky and LU factorization methods, can be adopted to simplify the matrix computation [28], [29]. The computation burden can then be noticeably reduced to $68 \cdot (2M + 2) + 3 \cdot (2M + 2)^2 = 1248$ multiplications and $51 \cdot (2M + 2) + 3 \cdot (2M + 2)^2 = 1044$ summations. Besides, increasing the window length has a very small effect on the total computation burden because it only increases the computation burden of RWT coefficients while the matrix dimension stays the same. Based on the analysis, one can see the total computation burden is fairly low. It can satisfy the time response requirement of time-critical applications.

IV. ELIMINATING DECAYING DC COMPONENT

Similar derivation procedures can be used to develop the algorithm for eliminating the effect of decaying dc offset. Let us consider the following signal model that contains the exponentially decaying component

$$y(n) = x(n) + A_\tau \cdot e^{-n\Delta T \cdot \tau}, \quad n = 0, 1, 2, \dots$$

where $x(n)$ is the signal model defined in (5), A_τ , and τ represents the amplitude and time constant of dc offset, respectively.

Applying RWT in scale a to represent signal $y(n)$ in the time-frequency domain as derived in the Appendix, we have

$$W_{y(n)}(a, k) = W_{x(n)}(a, k) + u_\tau(a, \tau, k) \cdot x_\tau(k) \quad k = 0, 1, \dots \quad (12)$$

From (12), one can see that the wavelet coefficient $W_{y(n)}$ contains the coefficient for signal $x(n)$ and the weighted decaying dc component. Since the time constant is unknown to u_τ , iterations are required to approximate it.

Let $\tilde{\tau}$ represent the initial estimate and rewrite (14a) (in the Appendix) by using the first-order Taylor series expansion, and we have

$$u_\tau(a, \tau, k) = u_\tau(a, \tilde{\tau}, k) + \left. \frac{du_\tau}{d\tau} \right|_{\tilde{\tau}} \cdot \Delta\tau = u_\tau(a, \tilde{\tau}, k) + u_\tau^1(a, \tilde{\tau}, k) \cdot \Delta\tau \quad (14b)$$

where $u_\tau^1(a, \tilde{\tau}, k) = -\sqrt{a}\Delta T^2 \sum_{l=k/a}^0 l \cdot e^{-al\Delta T \cdot \tau} \cdot Q$.

For simplicity, denote $u_\tau(a, \tilde{\tau}, k)$ and $u_\tau^1(a, \tilde{\tau}, k)$ as \tilde{u}_τ and \tilde{u}_τ^1 , respectively, and rewrite the above formula

$$u_\tau(a, \tau, k) = \tilde{u}_\tau + \tilde{u}_\tau^1 \cdot \Delta\tau.$$

Then, (12) can be expressed as follows:

$$W_{y(n)}(a, k) = \sum_{m=1}^M [\tilde{u}_m^c \cdot \tilde{x}_m^c(k) + \tilde{u}_m^{c1} \cdot \tilde{x}_m^{c1}(k)] + \sum_{m=1}^M [\tilde{u}_m^s \cdot \tilde{x}_m^s(k) + \tilde{u}_m^{s1} \cdot \tilde{x}_m^{s1}(k)] + \tilde{u}_\tau \cdot \tilde{x}_\tau(k) + \tilde{u}_\tau^1 \cdot \tilde{x}_\tau^1(k) \quad (15a)$$

where $\tilde{x}_\tau^1 = \tilde{x}_\tau \cdot \Delta\tau$

Applying RWT to $y(n)$ in a series of scales $a_1, a_2, \dots, a_{4M+2}$, we obtain a series of coefficients $w_1, w_2, \dots, w_{4M+2}$ that can be expressed as the matrix, shown at the bottom of the page. For simplicity, we represent the above matrix in vector form. At sample k , we have the following equation:

$$W'(k) = \tilde{U}'(k) \cdot \tilde{X}'(k). \quad (15b)$$

In (15b), the wavelet coefficient $W'(k)$ can be calculated by using recursive (4). For weighting factor $\tilde{U}'(k)$, it can be calculated with approximate frequency \tilde{f}_m and time constant $\tilde{\tau}$ by using (8a)–(8b), (9a)–(9b), and (14a)–(14b), respectively. Solving matrix (15b), we obtain the vector variable $\tilde{X}'(k)$. Then, we can derive the formula to estimate $\Delta\tau$

$$\Delta\tau = \frac{\tilde{x}_\tau^1(k)}{\tilde{x}_\tau(k)}. \quad (16a)$$

And (11a) can be used to estimate Δf_m . After we obtain the time constant and frequency adjustments, update those two variables with $\tilde{f}_m + \Delta f_m$ and $\tilde{\tau} + \Delta\tau$, and iterate the above approximation procedures until either the changes of variables reach the cutoff value or a maximum number of iterations is performed. As a result, the real frequency and time constant can be estimated at the last iteration. Then, the amplitude A_m and phase angle φ_m can be estimated by using (11b) and (11c), respectively. If we approximate the exponential function by using the second-order Taylor expansion, we obtain

$$x_\tau(k) = A_\tau \cdot e^{-k\Delta T \cdot \tau} = A_\tau \cdot \left[1 - k\Delta T \cdot \tau + \frac{1}{2}(k\Delta T \cdot \tau)^2 \right].$$

$$\begin{bmatrix} w_{a_1} \\ w_{a_2} \\ \vdots \\ w_{a_{4M}} \\ w_{a_{4M+1}} \\ w_{a_{4M+2}} \end{bmatrix} = \begin{bmatrix} \tilde{u}_{1,a_1}^c & \tilde{u}_{1,a_1}^{c1} & \dots & \tilde{u}_{M,a_1}^{s1} & \tilde{u}_{\tau,a_1} & \tilde{u}_{\tau,a_1}^1 \\ \tilde{u}_{1,a_2}^c & \tilde{u}_{1,a_2}^{c1} & \dots & \tilde{u}_{M,a_2}^{s1} & \tilde{u}_{\tau,a_2} & \tilde{u}_{\tau,a_2}^1 \\ \vdots & \vdots & \ddots & \vdots & \vdots & \vdots \\ \tilde{u}_{1,a_{4M}}^c & \tilde{u}_{1,a_{4M}}^{c1} & \dots & \tilde{u}_{M,a_{4M}}^{s1} & \tilde{u}_{\tau,a_{4M}} & \tilde{u}_{\tau,a_{4M}}^1 \\ \tilde{u}_{1,a_{4M+1}}^c & \tilde{u}_{1,a_{4M+1}}^{c1} & \dots & \tilde{u}_{M,a_{4M+1}}^{s1} & \tilde{u}_{\tau,a_{4M+1}} & \tilde{u}_{\tau,a_{4M+1}}^1 \\ \tilde{u}_{1,a_{4M+2}}^c & \tilde{u}_{1,a_{4M+2}}^{c1} & \dots & \tilde{u}_{M,a_{4M+2}}^{s1} & \tilde{u}_{\tau,a_{4M+2}} & \tilde{u}_{\tau,a_{4M+2}}^1 \end{bmatrix} \cdot \begin{bmatrix} \tilde{x}_1^c \\ \tilde{x}_1^{c1} \\ \vdots \\ \tilde{x}_M^{s1} \\ \tilde{x}_\tau \\ \tilde{x}_\tau^1 \end{bmatrix}$$

The formula for estimating the magnitude of the decaying dc component is

$$A_\tau = \frac{\tilde{x}_\tau(k)}{1 - k\Delta T \cdot \tilde{\tau} + \frac{1}{2}(k\Delta T \cdot \tilde{\tau})^2}. \quad (16b)$$

The initial estimate of the time constant $\tilde{\tau}$ can be selected from a wide range: a half cycle to five cycles [15]. Generally, we select two cycles as the initial estimate. The expression for x_τ is given in (13). Given the sampling rate N and window size $1/4$ cycle, the (13) can be rewritten as $x_\tau = A_\tau \cdot e^{-1/4d}$ ($\tau = f_0/d$, $f_0 = 60$ Hz) or $x_\tau = A_\tau \cdot e^{-1/d}$ (the window size is 1 cycle). Considering a typical range for the time constant variable of the decaying dc component ($d = [0.5, 5]$) x_τ would take on the range $0.61A_\tau - 0.95A_\tau$ or $0.14A_\tau - 0.82A_\tau$ (A_τ is the amplitude of the decaying dc component), respectively. One can see that the value of x_τ has the same level as its amplitude. Thus, the issues of noise and division by zero due to the small value can be avoided. The flowchart for performing the algorithm is similar to the one shown in Fig. 3 except for modifying the wavelet coefficients and weighting matrix and introducing time constant variables into the iteration loop.

V. PERFORMANCE EVALUATION

In this section, the performance of the proposed estimation algorithm is fully evaluated with various test conditions covering static state, dynamic state, and transient state, and the results are compared with conventional DFT methods, improved DFT-based methods in [5]–[7], and the latest published techniques in [9], [10], [20], and [21]. In the static test, a signal model containing harmonics and noise is used and the performance is verified in a wide range of frequency deviations. The dynamic test uses the scenarios that may occur in the real power system. The scenarios including the frequency ramp, short-circuit fault, and power swing are simulated using appropriate signal models. In the transient test, three-phase current outputs from the Alternative Transients Program/Electromagnetic Transients Program (ATP/EMTP) [30] are used to verify the performance of eliminating the dc offset. All tests are performed with the sampling rate $N = 50$ samples per cycle, (i.e., $f_s = 3$ kHz, and data window size $l_s = 0.25$ cycle (12 samples)).

A. Static Test

A signal model containing harmonics and 0.1% (signal-to-noise ratio SNR = 60 dB) white noise is assumed, where $e(n)$ represents the zero-mean Gaussian noise. Let $A = 1.0$ p.u., $\varphi = 5^\circ$. The fundamental frequency f_1 varies over a wide range from 55 to 65 Hz in 0.2 Hz steps. Frequency error and total vector error (TVE) of the fundamental frequency component are estimated. Comparing to the DFT-based methods in [5]–[7], the algorithm can output the frequency and phasor parameters in about 4 ms. The method using three consecutive samples of the instantaneous signal in [9] and [10], denoted as MV, achieves the uncertainty of 10 million Hz. But they require a higher sampling frequency (6.4 kHz and higher) and the additional time delay (approximately two cycles) introduced by the band-pass filtering. The results are shown in Fig. 7. The output accuracy can be improved by extending the data window. Simulation results show that the maximum frequency error and TVE can be

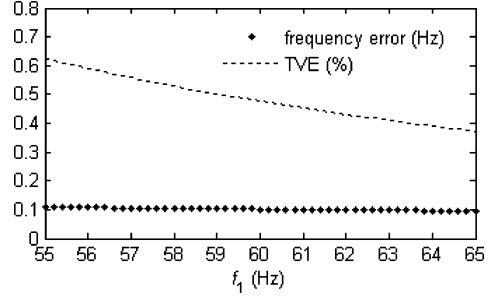


Fig. 7. Static test results using a quarter cycle data window.

TABLE I
TEST RESULTS FOR NOISE TESTS

Noise Level (SNR)	Window l_s (cycle)	RWT f_{Error} (Hz)	RWT TVE (%)	MV f_{Error} (Hz)
0.1% (60dB)	0.25	0.16	0.36	0.0043
	0.5	0.042	0.12	
	1.0	0.0029	0.036	
0.32% (50dB)	0.25	0.42	0.94	0.0076
	0.5	0.17	0.40	
	1.0	0.0051	0.064	
1% (40dB)	0.25	0.86	1.60	0.084
	0.5	0.35	1.08	
	1.0	0.068	0.26	
3.2% (30dB)	0.25	1.04	2.73	0.19
	0.5	0.58	1.59	
	1.0	0.10	0.68	

reduced to 0.05 Hz and 0.17%, respectively, when l_s is extended to a half cycle

$$x(n) = \sum_{m=1}^5 \frac{A}{m} \cos(2\pi \cdot m \cdot f \cdot n\Delta T + m \cdot \varphi) + e(n).$$

B. Noise Test

The inherent noise rejection capability of the algorithm is investigated by the noise test. The signal model for the static test is used. Let the fundamental frequency take the nominal value (60 Hz). For each level of the Gaussian noise, three data windows (quarter cycle, half cycle, and one cycle) were applied. The test was conducted by using the method MV except applying the variable data windows because the MV has a fixed size of data window. Each case was performed 10 times and the maximum value of the frequency estimate error for both RWT and MV, and TVE for RWT are shown in Table I. As one can expect, the better noise rejection can be obtained by slowing down the output response (i.e., prolonging the window span). The accuracy of RWT with one cycle window is in the same level with that of MV. The MV requires extra delay caused by filtering.

C. Dynamic Test

1) *Frequency Ramp*: The following synthesized sinusoidal signal with a frequency ramp is used to perform the frequency ramp tests

$$x(n) = A \cdot \cos(2\pi \cdot f \cdot n\Delta T + \pi \cdot df \cdot (n\Delta T)^2 + \varphi).$$

df is the frequency ramp rate. The signal frequency starts from 59 Hz followed by a positive ramp +10 Hz/s starting at 0.1 s

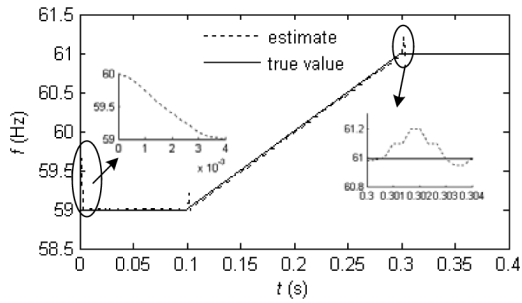


Fig. 8. Frequency ramp test results.

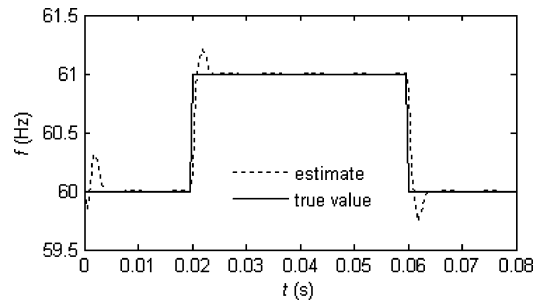


Fig. 11. Dynamic response for the frequency step.

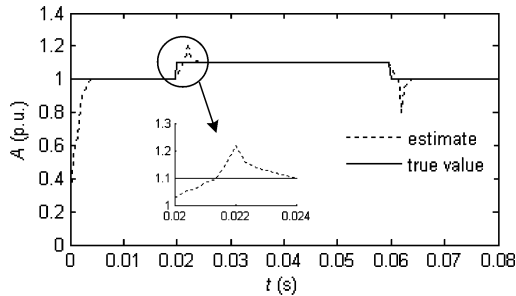


Fig. 9. Dynamic response for the amplitude step.

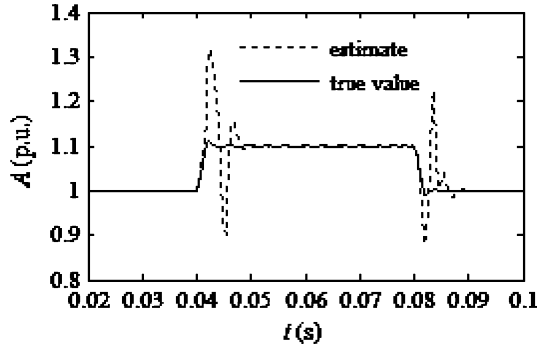


Fig. 12. Dynamic response for the amplitude step with prefiltering.

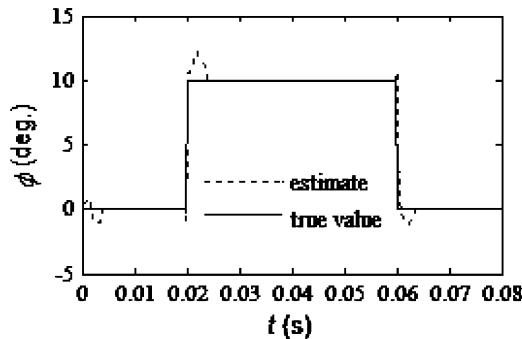


Fig. 10. Dynamic response for the phase-angle step.

and ending at 0.3 s, and then stays at 61 Hz for another 0.1 s. Fig. 8 shows the estimated frequencies and the true values. The transient behavior at the signal start and each discontinuity are shown as well. One can see that the outputs follow the inputs very closely and fast. The algorithm is able to output in about 4 ms with a quarter cycle window. The maximum error during ramp is 0.012 Hz. As discussed in the noise test, using more data can improve the tracking accuracy but results in the lower response as a tradeoff.

2) *Step Change*: To evaluate the dynamic response when exposed to an abrupt signal change, a positive step followed by a reverse step back to the starting value under various conditions is applied to the amplitude, phase angle, and frequency of a sinusoidal signal, respectively. Studies indicate that under all three types of steps that the algorithm shows similar dynamic behavior. The results of the amplitude step (10% of normal value), phase step ($\pi/18$ rad), and frequency step (1 Hz) are presented by Figs. 9–11, respectively. The steps occur at 0.02 and 0.06 s. One can observe that the outputs track the changes in inputs very fast.

To investigate the effect of prefiltering on the algorithm dynamic performance, a third-order Butterworth low-pass filter with a cutoff frequency of 320 Hz is used to process the input signals. Fig. 12 shows the result of the amplitude step test. Compared to Fig. 9, which shows the transient behavior without signal prefiltering, one can see that the low-pass filter enlarges the overshoot and undershoot, and slows the response from 4 to 10 ms though it is still faster than the DFT-based methods [5]–[7] and instantaneous sample-based methods [9], [10].

3) *Modulation*: A sinusoidal modulation signal model is used to simulate the transient progress of voltage and current signals during the power swing. Its amplitude and phase angle are applied with simultaneous modulation as shown in the following expression:

$$x(n) = A \cdot (1 + k_x \cos(2\pi \cdot f_a \cdot n\Delta T)) \cdot \cos(2\pi \cdot f \cdot n \cdot \Delta T + k_a \cos(2\pi \cdot f_a \cdot n\Delta T - \pi))$$

where f_a is the modulation frequency, k_x is the amplitude-modulation factor, and k_a is the phase-angle modulation factor. Equations (17a)–(17c) in the Appendix provide the true value of frequency, amplitude, and phase angle for the modulated signal model at output sample k .

Let $k_x = 0.1$, $k_a = 0.1$ radian and modulation frequency vary from 0.1 Hz to 2 Hz in a 0.1-Hz step. The results are compared to the instantaneous sample-based method MV. The mean of frequency deviation Δf_{mi} obtained by RWT and MV, and the mean m_i and standard deviation σ_i of the TVE by RWT in one second are calculated. Due to the limited space, only parts of test results are presented. As shown in Table II, the algorithm achieves good dynamic performance when exposed to signal oscillations.

TABLE II
TEST RESULTS FOR MODULATION TESTS

f_a (Hz)	RWT Δf_m (Hz)	MV Δf_m (Hz)	TVE (RWT)	
			m_i (%)	σ_i (%)
0.1	0.0018	0.0035	0.0070	0.0040
0.5	0.0218	0.0193	0.0805	0.0386
1.0	0.0538	0.0492	0.1612	0.0772
1.5	0.0857	0.1046	0.2417	0.1158
2.0	0.1178	0.1230	0.3227	0.1542

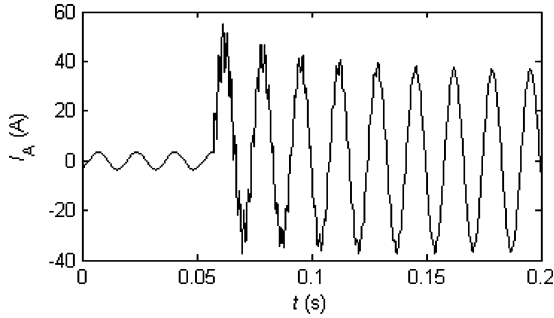


Fig. 13. Phase-A current waveform.

TABLE III
TEST RESULTS FOR DECAYING DC OFFSET

Filter	t_s (cycle)	I_A	I_B	I_C
		TVE (%)	TVE (%)	TVE (%)
FCDFD	5	0.9487	0.9559	0.9540
HCDFD	12.5	1.0156	1.0144	1.0166
LES	1.0	0.1082	0.1065	0.1062
SIM3	1.0	0.1129	0.1099	0.1118
HM	1.0	0.1202	0.1147	0.1174
RWT	0.75	0.1236	0.1145	0.1162

D. Transient Test

A 230 kV power network is modeled in EMTP to generate waveforms for testing the performance when eliminating decaying dc offset. A three-phase fault is applied and the three-phase currents are used as input signals. Fig. 13 shows the phase-A current waveform. One can see that the signal is contaminated with decaying dc component and high frequency noise during the beginning of postfault. The third-order Butterworth low-pass filter with a cutoff frequency of 320 Hz is used to attenuate the high-frequency components. Parameters estimation for the steady state (twenty cycles after the fault occurs) is used as a reference to measure the TVEs.

As shown in Table III, the results are compared with the conventional full-cycle DFT (FCDFD), half-cycle DFT (HCDFD) methods, least error square method (LES), simplified algorithm (SIM3) in [21], and hybrid method (HM) in [20]. In Table III, t_s is the time (in cycles) when the TVEs are measured. For the high accuracy, the algorithm was adjusted to a three-quarter cycle window span. The results show that the accuracy is comparable to those of LES, SIM3, and HM methods while the proposed algorithm requires a shorter data window, which results in faster response.

VI. CONCLUSIONS

This paper proposes a new wavelet function and its recursive wavelet transform. The method allowing real-time estimating of power system frequency, magnitude and phase while eliminating the impact of decaying dc component based on RWT is proposed. The algorithm features rapid response and accurate results over a wide range of frequency deviations. It uses only a quarter cycle of input signals for outputting frequency, and magnitude and phase results for a signal contaminated with harmonics. The sampling rate and observation window size can be chosen to meet selected applications requirements. The analysis of the algorithm convergence characteristics indicates that the higher the sampling rate, the shorter the computation data window and the faster the rate the method outputs phasor, and vice-versa. The decaying dc component can be completely removed by estimating its parameters using RWT. The performance of the proposed algorithm is evaluated under a variety of conditions including static state, dynamic state, and transient state. Comparing other techniques results demonstrates the advantages. Computation burden analysis indicates that the computation requirement is moderate. Thus, this approach can satisfy the time-critical demand of the real-time applications in power systems.

APPENDIX

The RWT coefficient of a given signal $x(n)$ is expressed as

$$\begin{aligned}
 W_{x(n)}(a, k) &= \frac{\Delta T}{\sqrt{a}} \cdot \sum_{n=0}^k x(n) \cdot \psi^* \left(\frac{n-k}{a} \Delta T \right) \\
 k &= 0, 1, 2, \dots \\
 &= \frac{\Delta T}{\sqrt{a}} \cdot \sum_{n=0}^k \sum_{m=1}^M A_m \cos(2\pi f_m \cdot n \Delta T + \varphi_m) \\
 &\quad \cdot \left[\frac{\sigma}{2} \left(\frac{n-k}{a} \right) \Delta T + \frac{\sigma^2}{2} \left(\frac{n-k}{a} \right)^2 \cdot \Delta T^2 \right. \\
 &\quad \left. + \frac{\sigma^3}{3} \left(\frac{n-k}{a} \right)^3 \cdot \Delta T^3 \right] \\
 &\quad \cdot e^{(\sigma - j\omega_0) \cdot (n-k/a) \Delta T}.
 \end{aligned}$$

Denoting $n = l \cdot a + k$, $l \in [-k/a, 0]$, we have

$$\begin{aligned}
 W_{x(n)}(a, k) &= \frac{\Delta T}{\sqrt{a}} \cdot \sum_{l=-k/a}^0 \sum_{m=1}^M A_m \\
 &\quad \times \cos(2\pi f_m k \Delta T + \varphi_m + 2\pi f_m a \cdot l \Delta T) \\
 &\quad \cdot \left[\frac{\sigma}{2} (l \Delta T) + \frac{\sigma^2}{2} (l \Delta T)^2 + \frac{\sigma^3}{3} (l \Delta T)^3 \right] \\
 &\quad \cdot e^{(\sigma - j\omega_0) \cdot l \Delta T}.
 \end{aligned}$$

Expanding the cosine part and rearranging the equation, we obtain

$$\begin{aligned}
 W_{x(n)}(a, k) &= \sum_{m=1}^M u_m^c(a, f_m, k) \cdot x_m^c(k) \\
 &\quad + \sum_{m=1}^M u_m^s(a, f_m, k) \cdot x_m^s(k)
 \end{aligned}$$

where

$$x_m^c(k) = A_m \cos(2\pi f_m k \Delta T + \varphi_m) \quad (7a)$$

$$x_m^s(k) = A_m \sin(2\pi f_m k \Delta T + \varphi_m) \quad (7b)$$

$$u_m^c(a, f_m, k) = \frac{\Delta T}{\sqrt{a}} \cdot \sum_{l=-k/a}^0 \cos(2\pi f_m a \cdot l \Delta T) \cdot Q \quad (8a)$$

$$u_m^s(a, f_m, k) = -\frac{\Delta T}{\sqrt{a}} \cdot \sum_{l=-k/a}^0 \sin(2\pi f_m a \cdot l \Delta T) \cdot Q$$

$$Q = \left[\frac{\sigma}{2} (l \Delta T) + \frac{\sigma^2}{2} (l \Delta T)^2 + \frac{\sigma^3}{3} (l \Delta T)^3 \right] \cdot e^{(\sigma - j\omega_0) \cdot l \Delta T} \quad (8b)$$

Similarly, for signal $y(n)$, we have the expression for the RWT coefficient

$$W_{y(n)}(a, k) = \frac{\Delta T}{\sqrt{a}} \cdot \sum_{n=0}^k y(n) \cdot \psi^* \left(\frac{n-k}{a} \Delta T \right),$$

$$k = 0, 1, 2, \dots$$

$$= W_{x(n)}(a, k) + \frac{\Delta T}{\sqrt{a}} \cdot \sum_{n=0}^k A_\tau \cdot e^{-n \Delta T \tau}$$

$$\times \left[\frac{\sigma}{2} \left(\frac{n-k}{a} \right) \Delta T + \frac{\sigma^2}{2} \left(\frac{n-k}{a} \right)^2 \cdot \Delta T^2 + \frac{\sigma^3}{3} \left(\frac{n-k}{a} \right)^3 \cdot \Delta T^3 \right] \cdot e^{(\sigma - j\omega_0) \cdot (n-k/a) \Delta T}.$$

Denoting $n = l \cdot a + k$, $l \in [-k/a, 0]$, we have

$$W_{y(n)}(a, k) = W_{x(n)}(a, k) + u_\tau(a, \tau, k) \cdot x_\tau(k)$$

where

$$x_\tau(k) = A_\tau \cdot e^{-k \Delta T \tau} \quad (13)$$

$$u_\tau(a, \tau, k) = \frac{\Delta T}{\sqrt{a}} \cdot \sum_{l=-k/a}^0 e^{-al \Delta T \tau} \cdot Q, \quad (14a)$$

The true value of frequency, amplitude, and phase angle at the output sample k for the modulated signal model can be computed as

$$f(k) = f_0 - k_a f_a \sin(2\pi \cdot f_a \cdot k \Delta T - \pi) \quad (17a)$$

$$X_m(k) = A \cdot (1 + k_x \cos(2\pi \cdot f_a \cdot k \Delta T)) \quad (17b)$$

$$\varphi(k) = k_a \cos(2\pi \cdot f_a \cdot k \Delta T - \pi). \quad (17c)$$

REFERENCES

- [1] A. G. Phadke and J. S. Thorp, *Computer Relaying for Power Systems*. New York: Wiley, 1988.
- [2] M. V. S. Yalla, "A digital multifunction protective relays," *IEEE Trans. Power Del.*, vol. 7, no. 1, pp. 193–201, Jan. 1992.
- [3] A. G. Phadke, T. Hlibka, and M. Ibrahim, "A digital computer system for EHV substation: Analysis and field tests," *IEEE Trans. Power App. Syst.*, vol. PAS-95, no. 1, pp. 291–301, Jan./Feb. 1976.
- [4] N. T. Stringer, "The effect of DC offset on current-operated relays," *IEEE Trans. Ind. Appl.*, vol. 34, no. 1, pp. 30–34, Jan./Feb. 1998.
- [5] T. S. Sidhu and M. S. Sachdev, "An iterative technique for fast and accurate measurement of power system frequency," *IEEE Trans. Power Del.*, vol. 13, no. 1, pp. 109–115, Jan. 1998.
- [6] G. Benmouyal, "An adaptive sampling interval generator for digital relaying," *IEEE Trans. Power Del.*, vol. 4, no. 3, pp. 1602–1609, Jul. 1989.
- [7] D. Hart, D. Novosel, Y. Hu, B. Smith, and M. Egoif, "A new frequency tracking and phasor estimation algorithm for generator protection," *IEEE Trans. Power Del.*, vol. 12, no. 3, pp. 1064–1073, Jul. 1997.
- [8] P. J. Moore, J. H. Allmeling, and A. T. Johns, "Frequency relaying based on instantaneous frequency measurement," *IEEE Trans. Power Del.*, vol. 11, no. 4, pp. 1737–1742, Oct. 1996.
- [9] M. D. Kusljevic, "Simultaneous frequency and harmonic magnitude estimation using decoupled modules and multirate sampling," *IEEE Trans. Instrum. Meas.*, vol. 59, no. 4, pp. 954–962, Apr. 2010.
- [10] A. Lopez, J. C. Montano, M. Castilla, J. Gutierrez, M. D. Borras, and J. C. Bravo, "Power system frequency measurement under nonstationary situations," *IEEE Trans. Power Del.*, vol. 23, no. 2, pp. 562–567, Apr. 2008.
- [11] A. A. Girgis and W. L. Peterson, "Adaptive estimation of power system frequency deviation and its rate of change for calculating sudden power system overloads," *IEEE Trans. Power Del.*, vol. 5, no. 2, pp. 585–594, Apr. 1990.
- [12] I. Kamwa and R. Grondin, "Fast adaptive schemes for tracking voltage phasor and local frequency in power transmission and distribution systems," in *Proc. IEEE Power Eng. Soc. Transm. Distrib. Conf.*, Dallas, TX, 1991, pp. 930–936.
- [13] K. M. El-Naggar and H. K. M. Youssef, "A genetic based algorithm for frequency relaying applications," *Elect. Power Syst. Res.*, vol. 55, no. 3, pp. 173–178, 2000.
- [14] L. L. Lai and W. L. Chan, "Real time frequency and harmonic evaluation using artificial networks," *IEEE Trans. Power Del.*, vol. 14, no. 1, pp. 52–57, Jan. 1999.
- [15] G. Benmouyal, "Removal of DC-offset in current waveforms using digital mimic filtering," *IEEE Trans. Power Del.*, vol. 10, no. 2, pp. 621–630, Apr. 1995.
- [16] J.-C. Gu and S.-L. Yu, "Removal of DC offset in current and voltage signals using a novel Fourier filter algorithm," *IEEE Trans. Power Del.*, vol. 15, no. 1, pp. 73–79, Jan. 2000.
- [17] J.-Z. Yang and C.-W. Liu, "Complete elimination of DC offset in current signal for relaying applications," in *Proc. IEEE Power Eng. Soc. Winter Meeting*, Jan. 2000, vol. 3, pp. 1933–1938.
- [18] T. S. Sidhu, X. Zhang, F. Albasri, and M. S. Sachdev, "Discrete-Fourier-transform-based technique for removal of decaying DC offset from phasor estimates," *Proc. Inst. Elect. Eng., Gen., Transm. Distrib.*, vol. 150, no. 6, pp. 745–752, Nov. 2003.
- [19] S. H. Kang, D. G. Lee, S. R. Nam, P. A. Crossley, and Y. C. Kang, "Fourier transform-based modified phasor estimation method immune to the effect of the DC offsets," *IEEE Trans. Power Del.*, vol. 24, no. 3, pp. 1104–1111, Jul. 2009.
- [20] S. R. Nam, J. Y. Park, S. H. Kang, and M. Kezunovic, "Phasor estimation in the presence of DC offset and ct saturation," *IEEE Trans. Power Del.*, vol. 24, no. 4, pp. 1842–1849, Oct. 2009.
- [21] Y. Guo and M. Kezunovic, "Simplified algorithms for removal of the effect of exponentially decaying DC-offset on the Fourier algorithms," *IEEE Trans. Power Del.*, vol. 18, no. 3, pp. 711–717, Jul. 2003.
- [22] C.-S. Yu, "A discrete Fourier transform-based adaptive mimic phasor estimator for distance relaying applications," *IEEE Trans. Power Del.*, vol. 21, no. 4, pp. 1836–1846, Oct. 2006.
- [23] O. Chaari, M. Meunier, and F. Brouaye, "Wavelets: A new tool for the resonant grounded power distribution systems relaying," *IEEE Trans. Power Del.*, vol. 11, no. 3, pp. 1301–1308, Jul. 1996.
- [24] C. Zhang, Y. Huang, X. Ma, W. Lu, and G. Wang, "A new approach to detect transformer inrush current by applying wavelet transform," in *Proc. POWERCON*, Aug. 1998, vol. 2, pp. 1040–1044.
- [25] X.-N. Lin and H.-F. Liu, "A fast recursive wavelet based boundary protection scheme," in *Proc. IEEE Power Eng. Soc. Gen. Meeting*, Jun. 2005, vol. 1, pp. 722–727.
- [26] M. Stephane, *A Wavelet Tour of Signal Processing*, 3rd ed. London, U.K.: Academic Press, 2008.
- [27] *IEEE Standard for Synchrophasors for Power Systems*, IEEE Std. C37.118-2005, Mar. 2006.
- [28] A. Abur and A. G. Exposito, *Power System State Estimation*, 1st ed. Boca Raton, FL: CRC, 2004.
- [29] A. R. Bergen and V. Vittal, *Power Systems Analysis*, 2nd ed. Upper Saddle River, NJ: Prentice-Hall, 1999.

- [30] Power Syst. Relay. Committee, EMTP reference models for transmission line relay testing report. 2001. [Online]. Available: <http://www.pes-psrc.org>

Jinfeng Ren (S'07) received the B.S. degree from Xi'an Jiaotong University, Xi'an, China, in 2004, and is currently pursuing the Ph.D. degree at Texas A&M University, College Station, TX.

His research interests are new algorithms and test methodology for synchrophasor measurements and their applications in power system protection and control as well as new digital signal-processing techniques for power system measurement and instrumentation, and automated simulation methods for multifunctional intelligent electronic devices testing.

Mladen Kezunovic (S'77–M'80–SM'85–F'99) received the Dipl. Ing., M.S., and Ph.D. degrees in electrical engineering in 1974, 1977, and 1980, respectively.

Currently, he is the Eugene E. Webb Professor and Site Director of the Power Engineering Research Center (PSerc), a National Science Foundation I/UCRC at Texas A&M University, College Station, TX. He was with Westinghouse Electric Corp., Pittsburgh, PA, from 1979 to 1980 and the Energoinvest Company, Europe, from 1980 to 1986, and spent a sabbatical at EdF, Clamart, France, from 1999 to 2000. He was also a Visiting Professor at Washington State University, Pullman, from 1986 to 1987 and The University of Hong Kong in 2007. His main research interests are digital simulators and simulation methods for intelligent electronic device testing as well as the application of intelligent methods to power system monitoring, control, and protection.

Dr. Kezunovic is a member of CIGRE and a Registered Professional Engineer in Texas.